Universiteit Antwerpen

This item is the archived peer-reviewed author-version of:

# Phase problem in the B-site ordering of $La_2CoMnO_6$ : impact on structure and magnetism

**Reference:**

Egoavil Escobar Ricardo Juan, Huehn S., Jungbauer M., Gauquelin Nicolas, Béché Armand, van Tendeloo Gustaaf, Verbeeck, Moshnyaga V..- Phase problem in the B-site ordering of $La_2CoMnO_6$ : impact on structure and magnetism
Nanoscale / Royal Society of Chemistry - ISSN 2040-3364 - 7:21(2015), p. 9835-9843
DOI: http://dx.doi.org/doi:10.1039/c5nr01642h
Handle: http://hdl.handle.net/10067/1264230151162165141

uantwerpen.be

Institutional repository IRUA

# Phase problem in the B-site Ordering of $La_2CoMnO_6$: Impact on Structure and Magnetism

R. Egoavil[2], S. Hühn[1], M. Jungbauer[1], N. Gauquelin[2], A. Béché[2], G. Van Tendeloo[2], J. Verbeeck[2], V. Moshnyaga[1]

[1]*Erstes Physikalisches Institut, Universität Göttingen, Friedrich-Hund-Platz 1, 37077 Göttingen, Germany*

[2]*EMAT, University of Antwerp, Groenenborgerlaan 171, 2020 Antwerp, Belgium*

Epitaxial double perovskite $La_2CoMnO_6$ (LCMO) films were grown by metalorganic aerosol deposition on $SrTiO_3$(111) substrates. A high Curie temperature, $T_C$ = 226 K, and large magnetization close to saturation, $M_S$(5 K) = 5.8 $\mu_B$/f.u., indicate a 97% degree of B-site (Co,Mn) ordering within the film. The Co/Mn ordering was directly imaged at the atomic scale by scanning transmission electron microscopy with energy-dispersive X-ray spectroscopy (STEM-EDX). Local electron-energy-loss spectroscopy (EELS) measurements reveal that the B-sites are predominantly occupied by $Co^{2+}$ and $Mn^{4+}$ ions in quantitative agreement with magnetic data. Relatively small values of the $(1/2\ 1/2\ 1/2)$ superstructure peak intensity, obtained by X-ray diffraction (XRD), point out the existence of ordered domains with an arbitrary phase relationship across the domain boundary. The size of these domains is estimated to be in the range 35-170 nm according to TEM observations and modelling the magnetization data. These observations provide important information towards the complexity of the cation ordering phenomenon and its implications on magnetism in double perovskites, and similar materials.

***Introduction.***

Double perovskites with general formula $A_2BB'O_6$ (A=La, Sr, Ca, B/B'=Co/Mn or Fe/Mo) are of great interest as ferromagnetic insulators and multiferroic materials as well as half-metallic ferrimagnets with high transition temperature. Their electronic properties depend crucially on the size and charge of the B-site cations, as well as on the degree of B-site ordering [1, 2, 3, 4]. In an ideally B-site ordered double perovskite the B and B' cations form sequences of B-O-B' chains,

while an order-reduced or disordered state is associated with a random distribution of B and B' cations with B-O-B, B-O-B' and B'-O-B' chains. For example $Sr_2FeMoO_6$ behaves as a ferrimagnetic metal in the ordered state and as an insulator in the disordered state [5]. A rock-salt ordering of B- and B'-cations, the most common type of ordering for ordered double perovskites, is stabilized for transition metal ions having an oxidation state difference of two and more, e.g. $Fe^{3+}/Mo^{5+}$ [1, 5].

More recently, the double perovskites $La_2MMnO_6$ (M=Co, Ni) are reported to exhibit ferromagnetic behavior and a magnetodielectric effect near room temperature [6, 7, 8, 9, 10, 11], making them a promising material for the next-generation of memory devices. A relatively high ferromagnetic Curie temperature ($T_C$) is found to be strongly dependent on the $M^{2+}$ and $Mn^{4+}$ cation ordering, as well as on the M-O-Mn superexchange interaction [9, 12, 13]. The synthesis of a nearly fully ordered phase in $La_2CoMnO_6$ was reported by Goodenough et. al [12] and Singh et. al [6, 7] by using high temperature and high oxygen pressure processing conditions. In spite of this progress, the achievement of a fully B-site ordered $Co^{2+}/Mn^{4+}$ phase still remains a challenge as disordered regions with low Tc, originating from e.g. oxygen vacancies, are often described [4, 12, 14-17]. It is commonly argued that ferromagnetism (FM) in the insulating $La_2CoMnO_6$ (LCMO) originates from the superexchange interaction between $Co^{2+}$ ions, having $3d^7$ configuration and half-filled $e_g$ orbitals with overall spin S=3/2, and $Mn^{4+}$ ions ($3d^3$, empty eg, S=3/2) [12]. Such FM superexchange due to the second Goodenough-Kanamori-Anderson rule results in a large theoretical saturation spin moment, $M_{sat}$ = 6 $\mu_B$/f.u. and a relatively high value of $T_C$ ~ 230 K. In the disordered LCMO the significantly lower $T_C$ ~ 130 K and smaller $M_{sat}$ ~ 4 $\mu_B$/f.u. were rationalized within the $Co^{3+}/Mn^{3+}$ vibronic superexchange interaction [12].

However, the correlation between the oxidation/spin state for Co and Mn ions in the ordered and disordered state is not fully understood [6, 14]. On the one hand, experiments by neutron scattering, X-ray absorption spectroscopy (XAS), X-ray magnetic circular dichroism and X-ray photoelectron spectroscopy of bulk- and nano-crystals have related the high-$T_C$ phase to the ordering of $Mn^{4+}$ and $Co^{2+}$ and the low-$T_C$ phase to the $Mn^{3+}/Co^{3+}$ disorder [4, 15, 16, 17, 18, 19, 20]. On the other hand, an XAS study on thin films by Wadati et. al [13] revealed a $Co^{2+}/Mn^{4+}$-originated electronic structure, which does not depend on the cation ordering. Up to date, no direct imaging of B-site ordering as well as no microscopic study of Mn/Co oxidation states in LCMO thin films was reported. Usually, the degree of Co/Mn ordering has been deduced

from the saturation magnetization and, more rarely, from X-ray diffraction (XRD) patterns; the latter should reveal a superstructure $(1/2\ 1/2\ 1/2)$ peak in the B-site ordered LCMO due to the doubling of the lattice parameter along the [111] axis. Together with the rock-salt B-site ordering this can be viewed as an infinite sequence of $(Mn\text{-}O/La\text{-}O/Co\text{-}O/La\text{-}O)_\infty$ atomic layers. The absence of local information on the cation ordering, quantified by direct measurements of the local electronic (chemical) structure, makes the fundamental research in double perovskites challenging and hinders their further development as promising materials for device applications.

Here we report epitaxial growth of double perovskite LCMO films by means of a metalorganic aerosol deposition (MAD) technique [21]. Being a chemical deposition route, MAD provides an attractive opportunity to grow films at conditions close to equilibrium, i.e. at high substrate temperatures, $T_{sub}$=800-1000°C, and high oxygen partial pressure, $p_{O2}$ ~ 0.2 atm, which both are thought to be helpful for the realization of B-site ordering [12, 17, 22, 23, 24]. The spatial distribution of the Co/Mn ordering in the film is examined by a detailed analysis of the electron diffraction pattern due the Co/Mn ordering and subsequently compared with direct chemical mapping of this ordering at the atomic scale by high-resolution STEM-EDX(EELS). The presence of ordered domains as well as the local Co and Mn electronic structure allowed us to provide insight into the origin of the magnetic properties of these films.

***Experimental details.***

$La_2CoMnO_6$ films with thicknesses, d=20-320 nm, were grown by MAD [20] on STO (111) substrates by using acetylacetonates of La, Mn and Co, dissolved in dimethylformamide. The substrate temperature was kept at T = 980°C and the growth and cooling rate were 10-20 nm/min and 50 K/min, respectively. XRD θ-2θ patterns in Bragg geometry with Cu $K_\alpha$ radiation were measured for global structural characterization. Local structure with atomic resolution was studied by means of high-angle annular dark-field (HAADF) scanning transmission electron microscopy (STEM), energy-loss-spectroscopy (EELS) and energy-dispersive X-ray spectroscopy (EDX), performed using an FEI Titan$^3$ microscope, equipped with aberration correctors for both image and probe forming lenses. To extend the field of view a 0.8 Å electron probe (21.4 mrad convergence semi-angle) was scanned over the specimen to obtain spatially resolved HAADF images of 8192x8192 pixels with a detector collecting scattered electrons in the

range 41.5 to 94.9 mrad (more details see "Supplementary Information"). The magnetization of the films was measured for temperatures, T = 5 to 400 K, and applied magnetic fields, H = 0 to 5 T, aligned in plane along the $[01\bar{1}]$ axis by using a Magnetic Properties Measurement System (MPMS) from Quantum Design.

***Results.***

In Fig. 1 an XRD pattern for a LCMO/STO (111) film with a thickness of d = 320nm, is shown. Along with the peaks, originating from the STO (111) substrate and some spurious reflections due to the not fully filtered $K_\beta$ and tungsten radiation (marked by stars in Fig. 1), one can see an out-of-plane epitaxy of the LCMO film with a pseudocubic lattice parameter, c = 3.875 Å. An impurity peak (marked by Imp in Fig. 1) can be attributed to a small amount of CoO and/or $CoMnO_3$ phases. Remarkably, the XRD pattern reveals the presence of the superstructure peaks at $2\theta = 19.9°$ and 62.3°, which show the ($\alpha_1$-$\alpha_2$) splitting, indicating a long-range-character of the crystal superstructure. Such lattice superstructures provide evidence for the doubling of the lattice parameter along the [111] direction. Considering the architecture of (111) planes, one can suggest that such doubling is caused by a rock-salt-like B-site ordering of Co/Mn ions. The obtained value of the XRD ordering parameter (see Fig. 1), $S = I(½½½)/I(111) = 1.1*10^{-3}$, was significantly smaller as that for perfectly ordered film, $S = 10^{-2}$ (see Suplementary Information), thus, signaling a far from perfect long range ordering. A large scale homogeneity of the prepared LCMO/STO (111) films was additionally illustrated by scanning tunneling microscopy and X-ray reflectivity (XRR) measurements (see Fig. SI4 of Supplementary Information), from which an LCMO/STO root mean squared (RMS) interface roughness, $\sigma_{i,RMS} \sim 1$ nm, and a surface roughness, $\sigma_{s,RMS} \sim 0.5$ nm, were obtained by fitting the XRR data with ReMagX [25].

Magnetic properties of a LCMO/STO(111) film with a thickness of ~320nm are shown in Fig. 2. A Curie temperature, $T_C$ = 226K, was evaluated from the minimum of the function, TCM=(1/M)*(dM/dT), where TCM is the temperature coefficient of the magnetization, M. A strong difference between field cooled (FC) and zero field cooled (ZFC) magnetization in an external field of H = 1kOe and in a wide temperature range T < 200 K (see Fig. 2a) indicates an inhomogeneous magnetic state, like cluster-glass, due to competitions between FM and antiferromagnetic (AFM) interactions [20, 26, 27]. The measured low temperature saturation

magnetization, $M_{sat}$(5K, 50kOe) ~ 5.8 $\mu_B$/f.u. and coercive field, $H_C$(5K) ~ 5kOe, agree well with data on the B-site ordered LCMO bulk samples or thin films reported previously in the literature [6, 7, 12, 22, 28]. It has to be considered that the relative error of $M_{sat}$ is about 5% and is mostly determined by the error in the calculation of the film volume. Moreover, it is evident that the shown hysteresis loop is still a minor loop and, hence, H = 50kOe is not sufficient to fully saturate the magnetization of the LCMO film.

The distribution of Co/Mn ordering or, in other words, the degree of long-range ordering over the whole LCMO (111) film with a thickness of ~320 nm was studied with atomically resolved HAADF imaging over large areas. Because of the very small (7.4%) difference in the scattering intensity between the heavier Co and the lighter Mn atom, we applied a Fourier filtering procedure to visualize the ordering within the whole film (see Fig. 3). The intensity of the $(1/2\ 1/2\ 1/2)$ and $(\overline{1/2}\ 1/2\ 1/2)$ superstructure reflections was used as a marker for the doubling of the cell parameter in the B-site ordered cell as shown in the inset of Fig. 3a). To compare with the XRD ordering parameter S, a normalized $(1/2\ 1/2\ 1/2)$/(111) intensity ratio map is presented in Fig. 3b. This is a numerical dark field intensity ratio map corresponding to the $(1/2\ 1/2\ 1/2)$ and (111) reflections. The brighter regions corresponding to high intensity of the superstructure peak represent B-site ordered regions and the darker regions with the lower superstructure peak intensity can be attributed to regions with an apparent reduction of ordering. Importantly, the superstructure peak was present in all studied regions, thus, suggesting that areas with reduced ordering (blue color) consist of the overlapped ordered domains having no fixed phase relation. Such overlapping reduces the apparent order seen in projection (see discussion below).

B-site ordering on the atomic scale was verified by EDX elemental maps of the La $L_\alpha$, Co $K_\alpha$, Mn $K_\alpha$, Sr $L_\alpha$, Ti $K_\alpha$ and O $K_\alpha$ excitation peaks taken from two regions of the film, i.e. ordered and apparently disordered. The combined color map, shown in Fig. 4 (Mn: red, Co: green and La: blue) shows a direct image of the Co/Mn layered ordering (Fig. 4 “Ordered” panel), while in the disordered region, mostly near the film/substrate interface, the Co and Mn atoms seem to be randomly distributed (Fig. 4 “Disordered” panel). Atomically resolved elemental EELS maps of the Co-$L_{2,3}$, Mn-$L_{2,3}$, La-$M_{4,5}$ and O-K edges further confirm the directly observed Co/Mn ordering (see Fig. SI1 of Supplementary Information).

To further investigate the local electronic structure, a high resolution EELS focused on the fine structure of the Mn-$L_{2,3}$, Co-$L_{2,3}$ and O-K edges was performed in both ordered and disordered regions as shown in Fig. 5. To estimate the valence of Mn and Co ions the experimental core loss spectral signatures were compared with high resolution EELS reference spectra, taken from bulk samples of $Mn_2O_3$ and $MnO_2$ for the Mn-$L_{2,3}$ and from CoO and $Co_2O_3$ samples for the Co-$L_{2,3}$ edges, collected under similar conditions. Remarkably, the Co and Mn signatures, observed in the spectra for the ordered region (pink curves), and the $Co^{2+}$ and $Mn^{4+}$ reference spectra are very similar. Indeed, the spectral shape and peak positions, indicated by arrows, resemble the reference spectra for $Co^{2+}$ with three characteristic peaks: a pre-peak at 775.7 eV, a major peak at 777.1 eV and a shoulder peak at 778.2 eV (Fig. 5f,h) and for $Mn^{4+}$ the pre-peak at 640.3 eV and the major peak at 642.7 eV (Fig. 5a,c), evidencing the presence of $Co^{2+}$ and $Mn^{4+}$ ions within the ordered region. In contrast, the spectra for the order-reduced region (blue curves) clearly deviate from those for $Co^{3+}$ and $Mn^{3+}$ references. Most interesting is that the main peak positions at 775.7 eV, 777.1 eV for Co and at 640.3 eV, 642.7 eV for Mn (indicated by arrows) are nearly identical to those obtained in the ordered region (only slight differences in spectral shape can be observed). For clarity, the Mn(Co) spectra is overlaid on each spectrum for both ordered and disordered domains with black arrows to indicate the corresponding spectral differences. For Mn, note (i) the slight broadening of the Mn-$L_3$ peak (the pre-peak intensity at 640.3 eV observed in the ordered domain is increased and broadened in the disordered domain indicating an increased transition probability towards lower energy losses) and (ii) the energy onset position in the disordered domain is slightly shifted ~0.37 eV towards the lower energy losses when compared with the ordered domain. For Co, note that (i) the pre-peak at 775.7 eV is less pronounced, (ii) the major peak is slightly shifted ~0.24 eV towards higher energy losses and (iii) the absence of the shoulder peak at 778.2 eV. The above-mentioned spectral differences would suggest the existence of intermediate valence states for Co and Mn in the disordered domain.

To get a quantitative estimation the experimentally measured Co- and Mn- spectral signatures for both ordered and order-reduced regions were fitted by a linear combination of the reference spectra for CoO, $Co_2O_3$ and $Mn_2O_3$, $MnO_2$, respectively, using the EELSMODEL software package [26, 27]. The obtained weights of ($Co^{2+}$/$Mn^{4+}$) were (99%/96.8%) and (90.1%/76.9%) for the ordered and order-reduced phases, respectively. In a second stage, the Co

and Mn spectral signatures were compared with multiplet calculations for a single $Co^{2+}$ and $Mn^{4+}$ state in octahedral coordination (Oh), by using slightly different crystal parameters in the order-reduced phase as compared to the ordered phase (black dashed-line in Fig. 5, for details see "Supplementary Information"). The multiplet calculations show a modification of the $t_{2g}$ and $e_g$ energy level states while the valence states of these elements should be preserved to $Co^{2+}$ and $Mn^{4+}$ to fit the experimental spectral signatures in the order-reduced LCMO phase. Furthermore, the fine structure spectra of the O-K edge acquired simultaneously for the ordered and order-reduced (disordered) regions present only minor differences (see Fig. SI3 of Supplementary Information).

If the regions with reduced ordering would be truly disordered, an average $Co^{2.5+}$ and $Mn^{3.5+}$ valence state would be expected, in disagreement with our experimental results. In fact in both ordered and order-reduced phases the $Co^{2+}/Mn^{4+}$ states are dominant proving that, indeed, local order exists even though the long range order prevents a direct visualization at atomic resolution in the order-reduced regions. Therefore, the valence states of the cobalt and manganese ions in the thin film are $Co^{2+}$ and $Mn^{4+}$ on a local scale, confirming the result of global XAS experiments reported by Wadati et al. [13].

***Discussion.***

The degree of short-range Co/Mn ordering, defined as the probability, p, that a Mn-ion has a Co-ion as a next neighbor, $0 < p < 1$, can be estimated indirectly from the measured saturation magnetization. Considering the theoretical value, $M_{sat}$ = 6 $\mu_B$/f.u., in a fully ordered $La_2Mn^{4+}Co^{2+}O_6$ with p = 1, the estimated degree of short-range ordering in our films with $M_{sat}$ ~ 5.8 $\mu_B$/f.u. is p ~ 0.97. This indicates that about 3% of B-site pairs in the LCMO lattice are Co/Co or Mn/Mn. Such defect pairs should account for the measured XRD ordering parameter, $S_{0.97} = 1.1*10^{-3}$ (see Fig. 1), which is significantly smaller than the theoretical value, $S_1 = 10^{-2}$, for a fully ordered LCMO (p=1), obtained from XRD simulations (see Supplementary information). In order to understand this apparent underestimation of the ordering parameter from XRD one needs to realize that the diffraction can be thought of as the interaction with a projected crystal potential. This projection is the reason why two overlapping domains with an out-of-phase ordering can

strongly reduce the measured ordering parameter even though a very high degree of ordering is locally present.

In order to further investigate this effect we note that in general, two types of defects in the otherwise ordered B-site matrix can exist: a) anti-site point defects (ASDs) and b) anti-phase boundaries (APBs). The ASDs yield a monotonic decrease of S and, thus, can hardly be responsible for the observed strong reduction of S for only 3% defect density. In contrast, APBs can result in a much larger reduction in S due to the projection argument discussed above. Indeed, a fully ordered LCMO (p=1) crystal phase with a volume V (Fig. 6a) will be separated into two phase-shifted B-site ordered crystalline domains with volumes V1 and V2. The resulting ordering parameter, $S = |V1-V2|/(V*S1)$, will be significantly reduced for V1~V2 and even goes to zero (V1=V2). Moreover, S would be strongly dependent on the distribution of the ordered and phase-shifted domains, yielding an arbitrary V1/V2 ratio and a strong variance of S as evidenced in Fig. 3.

APBs in an ordered double perovskite structure are previously reported to exist between the ordered domains [12]; they can alter the Co/Mn ordering in the LCMO film. However, in the MAD-grown LCMO film studied here, no extended antiphase boundaries were found with TEM. In contrast, a rather smooth transition between the ordered and disordered regions in Fig. 3b indicates the presence of irregularly shaped ordered domains, separated by a boundary region where (in projection) no ordering was detected. The disorder within these boundaries also destroys the long range order from one domain to the next which seems to be the reason for the reduced ordering parameter, S, observed in XRD and HAADF STEM. This concept is schematically illustrated in Fig. 6b. Hence, one has to consider the coexistence of ordered domains, accompanied by the reduced values, $S_{0.97} << S_1$, due to disturbed long range order, with a high saturation magnetization, $M_S = 5.8\ \mu_B$/f.u., inferring a 97% degree of short-range B-site ordering.

The study of the local electronic structure (see above) evidences that local $Co^{2+}/Mn^{4+}$ ordering exists even within the regions where the long range ordering is disturbed. The observed ordering map in Fig. 3, and the measured magnetization loop (Fig. 2b) can be linked together and rationalized within the existence of ordered domains. Namely, the maps presented in Fig. 3b)

show ordered domains with characteristic size of ~35-170 nm (purple color), intermixed with regions containing multiple domains (blue) leading to suppressed ordering, $S \lesssim 0$.

In addition, the presence of ordered anti-phase domains (APDs) can be correlated with the reduction of the low-field and remanent magnetization. Moreover, this is in line with the high saturation field H > 50kOe and the cluster-glass behavior due to AFM coupling between the different domains. Note, the M(H) is not closed even for the highest field (see Fig. 2b). In another double perovskite, $Sr_2FeMoO_6$, it was observed that the fully ordered FM crystallites, separated by APBs, are indeed AFM coupled [31], yielding the reduction of remanent magnetization, $M_R$, and an increase of coercive field, Hc. In LCMO, first-principle calculations exhibit the preference of an FM coupling of Mn-Mn antiphase defects driven by a double exchange [20]. However, it is not known how this will affect APB and, hence, we did not consider this in the following simplified model. In an applied magnetic field, H, the Zeeman energy of the FM domain, $E_{Zeeman}$, may exceed the magnetic surface energy of the AFM antiphase boundary, $E_{Surface}$, and the domain with antiparallel magnetization will flip along the field direction. For a cubic domain with the edge length, *a*, which consists of cubic unit cells with lattice constant, *c*, the relation between these two energies is given by:

$$E_{Surface} = 6a^2 J_{AFM}/c^2 = \mu_0 H a^3 M_{u.c.}/c^3 = E_{Zeeman}$$

Here $J_{AFM}$ is the AFM coupling energy per anti-phase boundary. Considering the value of LCMO magnetization/u.c., $M_{u.c} = 3\ \mu_B$, one gets for the domain size:

$$a = \frac{2\,cJ_{AFM}}{\mu_0 \mu_B} \times \frac{1}{H} \qquad (1)$$

$J_{AFM}$ can be roughly estimated in the case of $Mn^{4+}$-O-$Mn^{4+}$ AFM coupling from the Néel temperature, $T_N$~145K, [32] of $Ca_{0.8}Sr_{0.2}MnO_3$, which has the same average A-site ionic radius as $La^{3+}$ [33]. No perovskite material is available to estimate the $Co^{2+}$-O-$Co^{2+}$ AFM coupling. The external field to flip the biggest APD can be estimated from a simplified model, which assumes that all APDs are aligned parallel for H ~ 50kOe (see Fig. 7a). By decreasing the field, the magnetization of the domains will flip antiparallel to the applied field. According to Eq. 1 the smaller domains flip at a higher field than the bigger ones (see Fig. 7b) and all domains are AFM-coupled to the surrounding domains at H = 0 (see Fig. 7c), leading to $M_R(0) < M_S$. Apparently, the same value of $|M_R|$ will be restored under magnetization reversal for a definite (negative) field, which is marked by a red dot in M(H) loop of LCMO film in Fig. 7a. Assuming this

configuration is comparable with the zero-field state, $M_R(0)$, one can estimate the flip field of the largest APD to be $H_F$ ~ 10kOe (see Fig. 3b). Substituting this into Eq. 1 the estimated APD size, a~35-170 nm, corresponds well to the domain size, observed in TEM (Fig. 3b). For the lower boundary of "a" the maximal field, H = 50kOe, was taken which apparently seems to be very close to the saturation field.

***Summary.***

Epitaxial $La_2CoMnO_6$ films on STO(111) substrates were prepared by the MAD technique. B-site ordering in the film was directly imaged by atomically resolved STEM-EDX. The relatively small value of the XRD ordering parameter, S = I(½½½)/I(111) = $1.1*10^{-3}$, and the presence of regions with reduced Co/Mn ordering in the superstructure intensity map, obtained by spatially resolved HAADF-STEM imaging, are related to the presence of small ordered domains. Magnetization close to saturation, $M_S$ ~ 5.8 $\mu_B$/f.u., indicates a 97% of short-range B-site ordering. EELS measurements point out that the B-sites consist predominantly of $Co^{2+}$ and $Mn^{4+}$ both for ordered and for regions that appear to have a reduced order in projection in quantitative agreement with magnetic data. According to TEM and magnetization data the estimated size of the ordered domains is 35-170 nm. We believe the obtained results underscore the complexity of the cation ordering phenomenon and will help to understand and optimize the B-site ordering as well as the desirable properties of double perovskite thin films.

***Acknowledgements.***

Financial support by the Seventh Framework Programme (grant number 246102 IFOX) of the EU is acknowledged. J.V. acknowledges funding from the fund for scientific research Flanders: FWO project G.0044.13N ('Charge ordering'). The Titan microscope was partly funded by the Hercules fund from the Flemish Government. The authors acknowledge financial support from the European Union under the Seventh Framework Program under a contract for an Integrated Infrastructure Initiative. Reference No. 312483-ESTEEM.

***References.***


1. Woodward, G. & King, P. M., Cation ordering in perovskites. J. Mater. Chem. (20), 5785 (2010).
2. Anderson, M. T., Greenwood, K. B. & Taylor, P. K. R., B-cation arrangements in double perovskites. Progress in Solid State Chemistry (22), 197233 (1993).
3. Davies, P., Wu, H., Borisevich, A., Molodetsky, I. & Farber, L., Crystal Chemistry of complex perovskites: New cation-ordered dielectric oxides. Annu. Rev. Mater. Res. (38), 369401 (2008).
4. Krishna, M. J. & Venimadhav, A., Reentrant cluster glass behavior in $La_2CoMnO_6$ nanoparticles. J. of Appl. Phys. (113), 163906 (2013).
5. Serrate, D. & De Teresa, J. M. I. M. R., Double perovskites with ferromagnetism above room temperature. J. Phys.: Condens. Matter (19), 023201 (2007).
6. Singh, M. P., Truong, K. & Fournier, P., Magnetodielectric effect in double perovskite $La_2CoMnO_6$ thin films. Appl. Phys. Lett. (91), 042504 (2007).
7. Singh, M. P., Carpentier, S., Truong, K. & Fournier, P., Evidence of bidomain structure in double-perovskite $La_2CoMnO_6$ thin films. Appl. Phys. Lett. (90), 211915 (2007).
8. Lin, Y. Q. & Chen, X. M., Dielectric, ferromagnetic characteristics, and room-temperature magnetodielectric effects in double perovskite $La_2CoMnO_6$ ceramics. J. Am. Ceram. Soc. (94), 782-787 (2011).
9. Singh, M. P., Truong, K. D., Jandl, S. & Founier, P., Multiferroic double perovskites: Opportunities, issues, and challenges. J. Appl. Phys. (107), 09D917 (2010).
10. Zhu, M. et al., Electronic and magnetic properties of $La_2NiMnO_6$ and $La_2CoMnO_6$ with cationic ordering. Appl. Phys. Lett. (100), 062406 (2010).
11. Mandal, T. K., Felser, C., Greenblatt, M. & Kubler, J., Magnetic and electronic properties of double perovskites and estimation of their curie temperatures by ab initio calculations. Phys. Rev. B (78), 134431 (2008).
12. Dass, R. I. & B., G. J., Multiple magnetic phases of $La_2CoMnO_6$. Phys. Rev. B (67), 014401 (2003).
13. Wadati, H. et al., X-ray absorption studies of $La_2NiMnO_6$ and $La_2CoMnO_6$ thin films. Chemical & Materials Science (49), 114-115 (2009).

14. Baidya, S. & Saha-Dasgupta, T., Electronic structure and phonons in $La_2CoMnO_6$: A ferromagnetic insulator driven by coulomb-assisted spin-orbit coupling. Phys. Rev. B (84), 035131 (2011).
15. Bull, C. L., Gleeson, D. & Knight, K. S., Determination of B-Site ordering and structural transformations in the mixed transition metal perovskites $La_2CoMnO_6$ and $La_2NiMnO_6$. J. Phys.: Condens. Matter (15), 4927-4936 (2003).
16. Troyanchuk, I. O., Sazonov, A. P., Szymczak, H., Többens, D. M. & Gamari-Seale, H., Phase separation in $La_{2-x}A_xCoMnO_6$ (A=Ca and Sr) perovskites. J. of Exp. and Theo. Physics (99), 363 (2004).
17. Kyômen, T., Yamazaki, R. & Itoh, M., Correlation between magnetic properties and Mn/Co atomic order in $LaMn_{0.5}Co_{0.5}O_{3+\delta}$: I. Second-order nature in Mn/Co atomic ordering and valence state. Chem. Mater. (15), 4798-4803 (2003).
18. Burnus, T. et al., Local electronic structure and magnetic properties of $LaMn_{0.5}Co_{0.5}O_3$ studies by X-ray absorption and magnetic circular dichroism spectroscopy. Phys. Rev. B (77), 125124 (2008).
19. Joly, V. L. J., Khollam, Y. B., Joy, P. A., Gopinath, C. S. & Date, S. K., Unusual charge disproportionation and associated magnetic behaviour in nanocrystalline $LaMn_{0.5}Co_{0.5}O_3$. J. Phys.: Condens. Matter (13), 1100111007 (2001).
20. Bai Y., Xia Y., Li H., Han L., Wang Z., Wu X., Lv S., Lui X. and Meng J., A-Site-Doping Enhanced B-Site Ordering and Correlated Magnetic Property in $La_{2-x}Bi_xCoMnO6$, J. Phys. Chem. C 116 (32), 16841-16847 (2012).
21. Moshnyaga, V. et al., Preparation of rare-earth manganite-oxide thin films by metalorganic aerosol deposition technique. Appl. Phys. Lett. (74), 2842 (1999).
22. Gou, H. Z., Gupta, A., Zhang, J., Varela, M. & Pennycook, S. J., Effect of oxygen concentration on the magnetic properties of $La_2CoMnO_6$ thin films. Appl. Phys. Lett (91), 202509 (2007).
23. Truong, K. D., Laverdire, J., Singh, M. P., Jandl, S. & P., F., Impact of Co/Mn cation ordering on phonon anomalies in $La_2CoMnO_6$ double perovskites: Raman spectroscopy. Phys. Rev. B (76), 132413 (2007).
24. Kyômen, T., Yamazaki, R. & Itoh, M., Correlation between magnetic properties and Mn/Co atomic order in $LaMn_{0.5}Co_{0.5}O_{3+\delta}$: 2. Magnetic and calorimetric properties. Chem. Mater. (16), 179 (2004).

25. Macke, S., Brück, S., Audehm, P., Harlander, M. & Goering, E., ReMagX: X-ray Magnetic Reflectivity Tool, Available at www.mf.mpg.de/remagx.html (2009).
26. Wang X., James M., Horvat J. and Dou S., Spin glass behaviour in ferromagnetic $La_2CoMnO_6$ perovskite manganite, Supercond. Sci. Technol., vol. 15, 427-430 (2002).
27. Bai Y., Liu X., Xia Y., Li X., Deng X., Han L., Liang Q., Wu X., Wang Z. and Meng J., B-site ordered induced suppression of magnetic cluster glass and dielectric anomaly in $La_{2-x}Bi_xCoMnO_6$, Appl. Phys. lett. (100), 222907 (2012).
28. Barón-González, A. J., Frontera, C., Garcia-Muñoz, J. L., Roqueta, J. & Santiso, J., Magnetic structural properties and B-site order of two epitaxial $La_2CoMnO_6$ films with perpendicular out-of-plane orientation. J. of Phys.: Conf. Series (200), 092002 (2010).
29. Verbeeck, J. & van Aert, S., Model based quantification of EELS spectra. Ultramicroscopy (101), 207224 (2004).
30. Verbeeck, J. & van Aert, S., Available at www.eelsmodel.ua.ac.be.
31. Goodenough, J. B. & Dass, R. I., Comment on the magnetic properties of the system $Sr_{2-x}Ca_xFeMoO_6$. Int. J. of Inorg. Mat. 2, 3-9 (2000).
32. Chmaissem, O. et al., Relationship between structural parameters and the Néel temperature in $Sr_{1-x}Ca_xMnO_3$ ($0<x<1$) and $Sr_{1-y}Ba_yMnO_3$ ($y<0.2$). Phys. Rev. B 64, 134412 (2001).
33. Shannon, R. D., Revised effective ionic radii and systematic studies of interatomic distances in halides and chalcogenides. Acta Cryst. A32, 751-767 (1976).

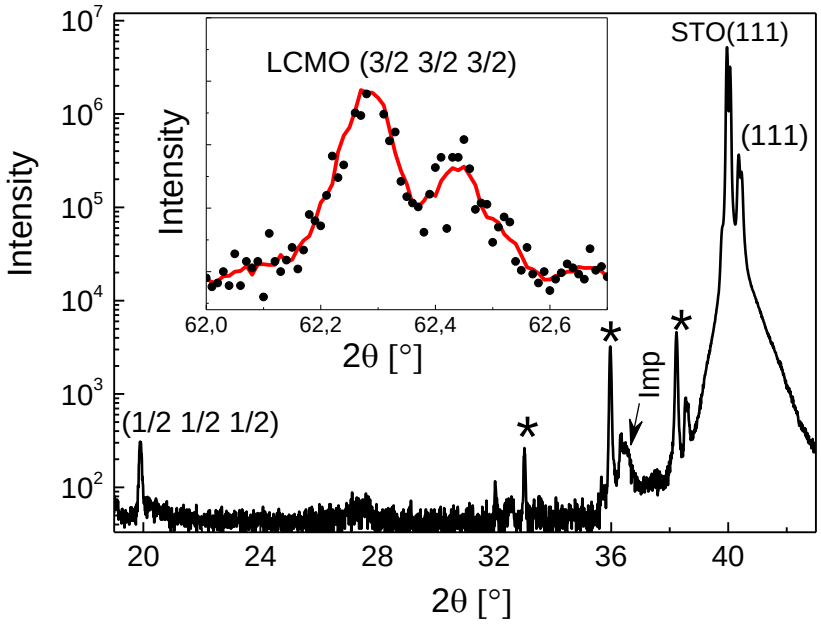


Fig. 1: a) XRD pattern of LCMO/STO(111) film with the thickness, d ~ 320 nm. The stars symbolize spurious reflexes due to not fully monochromatic Cu Kα. A small impurity peak is marked by "Imp". The inset shows the superstructure peak $(^3/_2\,^3/_2\,^3/_2)$ with $\alpha_1$-$\alpha_2$ splitting.

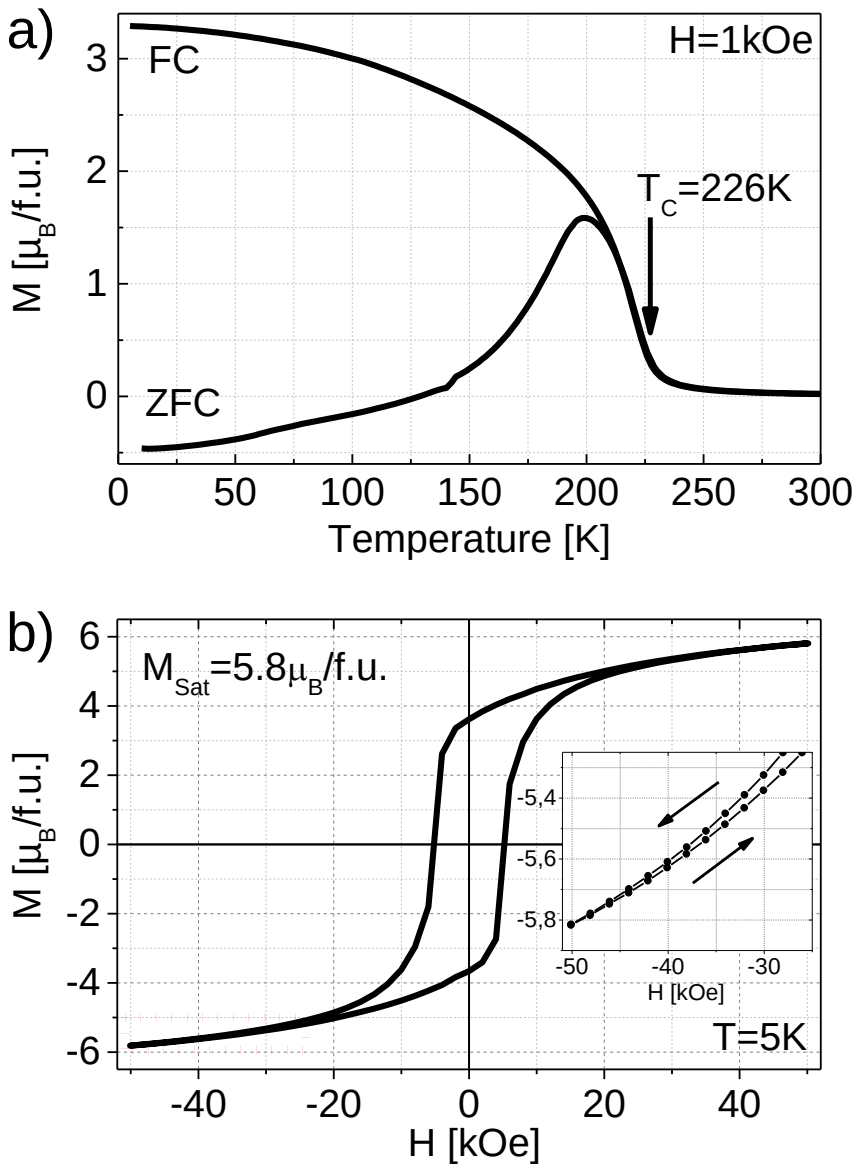


Fig. 2: a) The field cooled (FC) and zero field cooled (ZFC) magnetization vs temperature in an external field H = 1kOe for the B-site ordered LCMO with $T_C$ = 226 K. b) The M(H) loop at T = 5K with $M_{sat}$(50kOe) = 5.8 μB/f.u. The inset shows the magnified red marked area; apparently, M(H) is nonlinear and is not closed up to H = 50kOe.

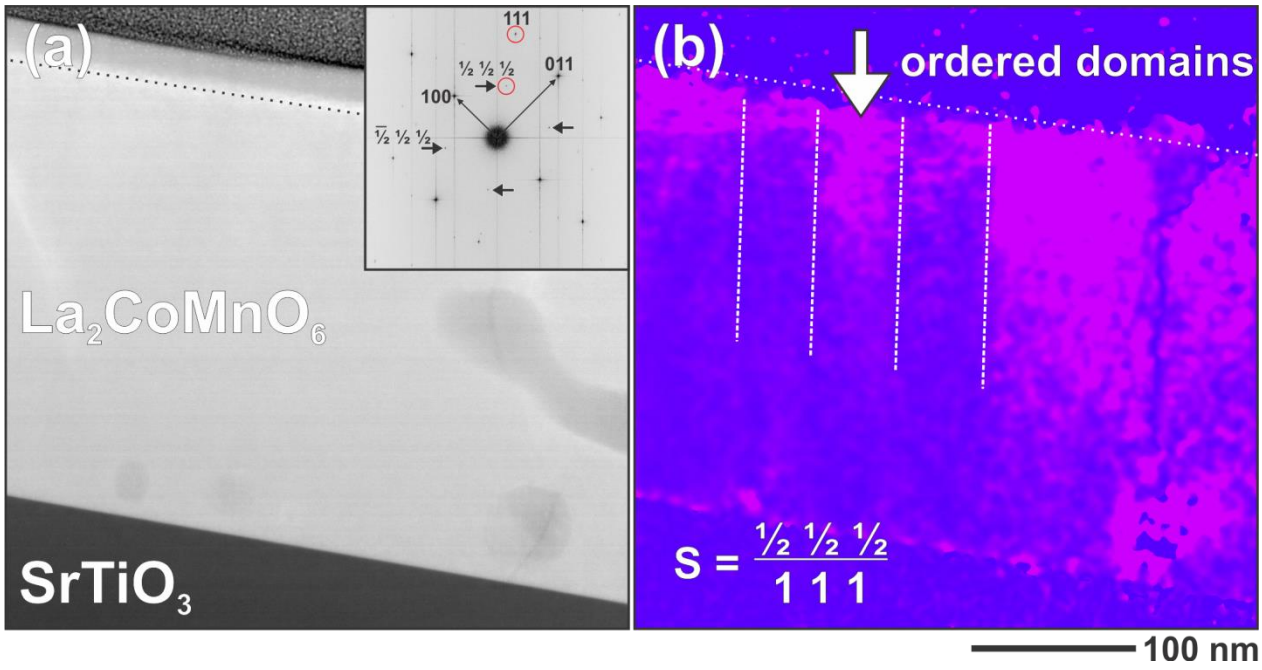


Fig. 3: (a) A high resolution 8192x8192 HAADF image of the film. Fourier filtering of the image in (a) with selected superstructure reflections marked by horizontal black arrows is shown as inset. (b) Numerical amplitude divided color map of the two $(^1/_2\,^1/_2\,^1/_2)$ and (111) reflections, respectively, showing the ordered (purple) and disordered (blue) domain regions.

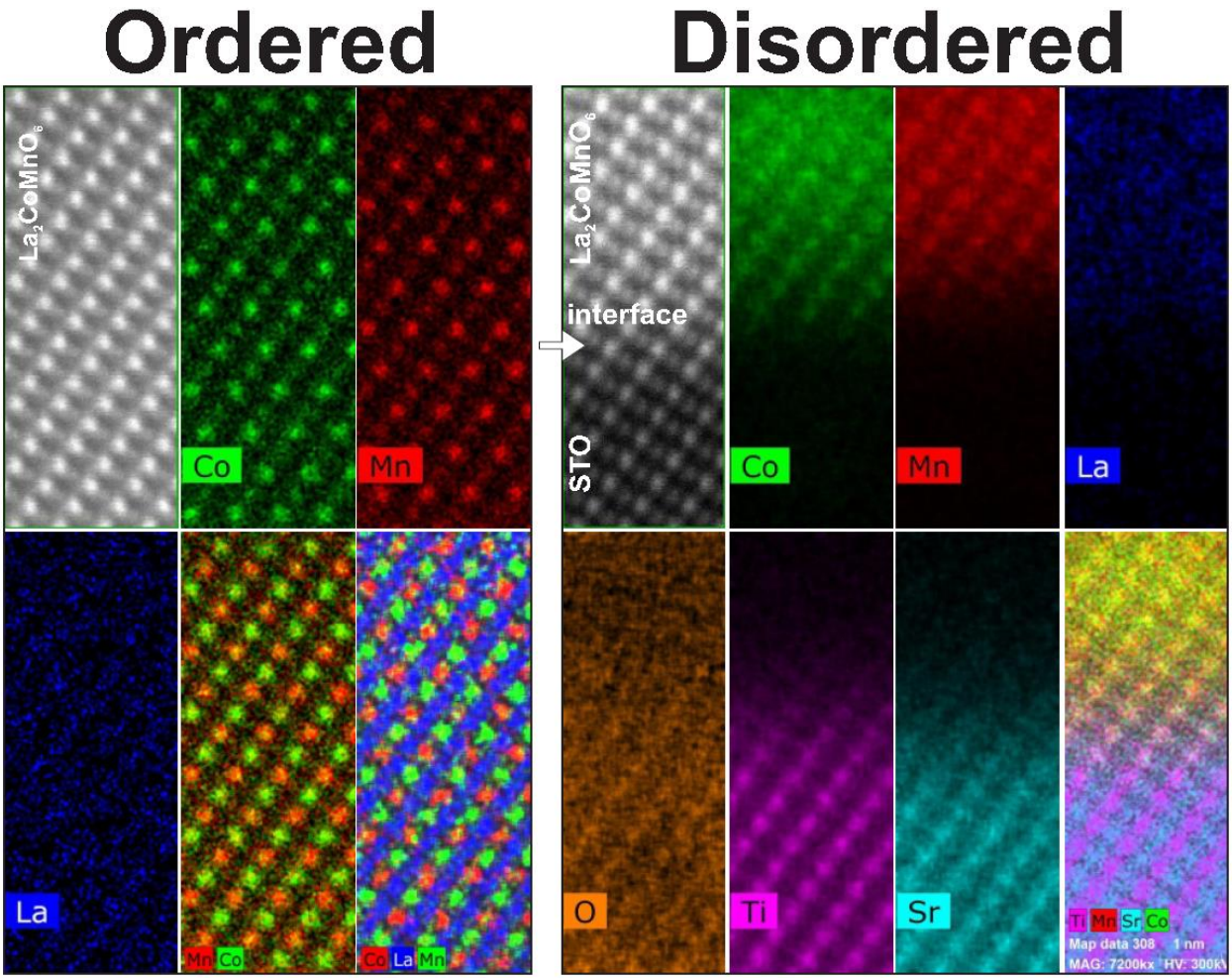


Fig. 4: Recorded atomic resolution HAADF image and its corresponding EDX and EELS maps of the ordered and disordered regions in a $La_2CoMnO_6$ double perovskite film. The combined color map with Co (green), Mn (red), La (blue), Sr (cyan), Ti (magenta) and O (orange) demonstrate the two different states.

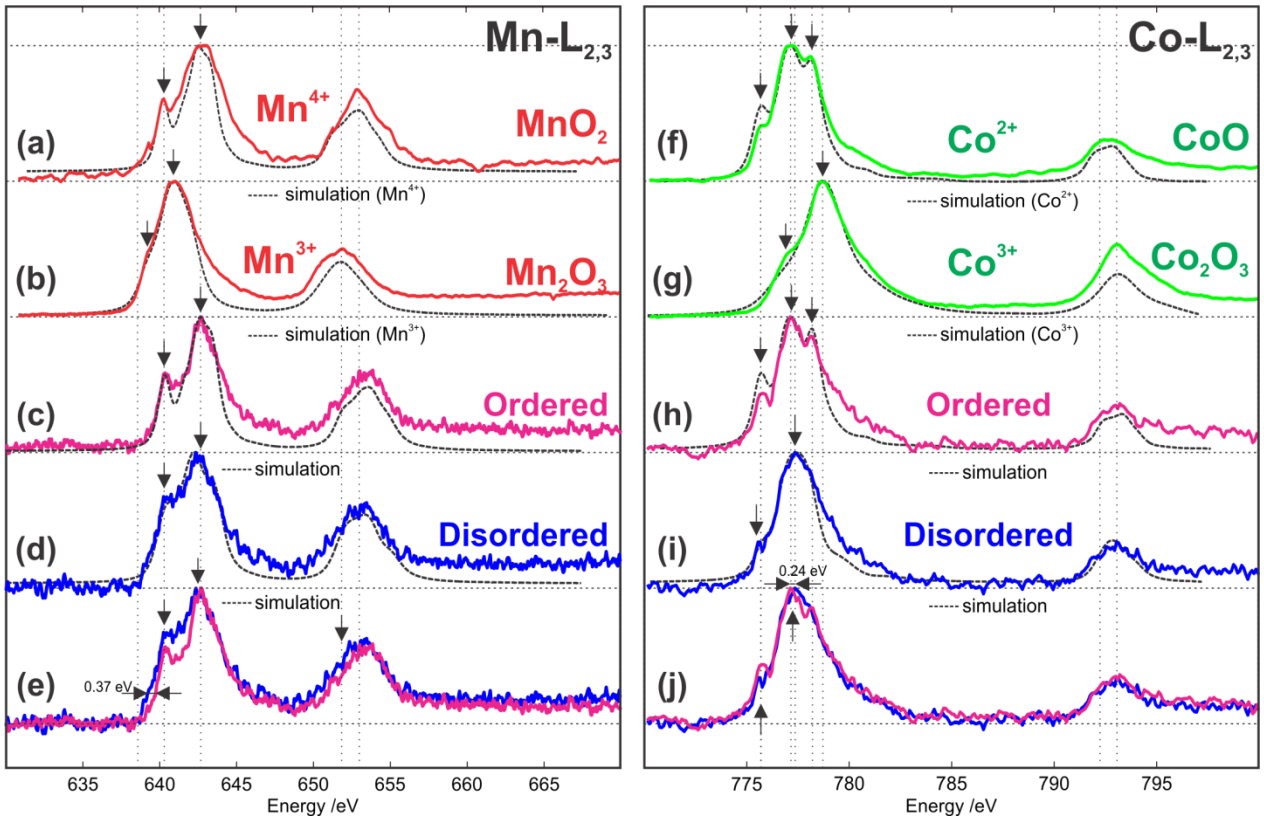


Fig. 5: ELNES of the B-site cations in a $La_2CoMnO_6$ thin film: (a,b & f,g) simulated and experimental reference of $Mn^{4+}$ (from $MnO_2$), $Mn^{3+}$ (from $Mn_2O_3$) and $Co^{2+}$ (from CoO), $Co^{3+}$ (from $Co_2O_3$) $L_{2,3}$ edge fine structures. (c,d & h,i) Mn-$L_{2,3}$ and Co-$L_{2,3}$ edge ELNES signatures from the ordered (pink) and the order-reduced (blue) region in the $La_2CoMnO_6$ film. (e,j) The overlaid Mn and Co spectra for both ordered and disordered domains with black arrows to indicate the corresponding spectral differences.

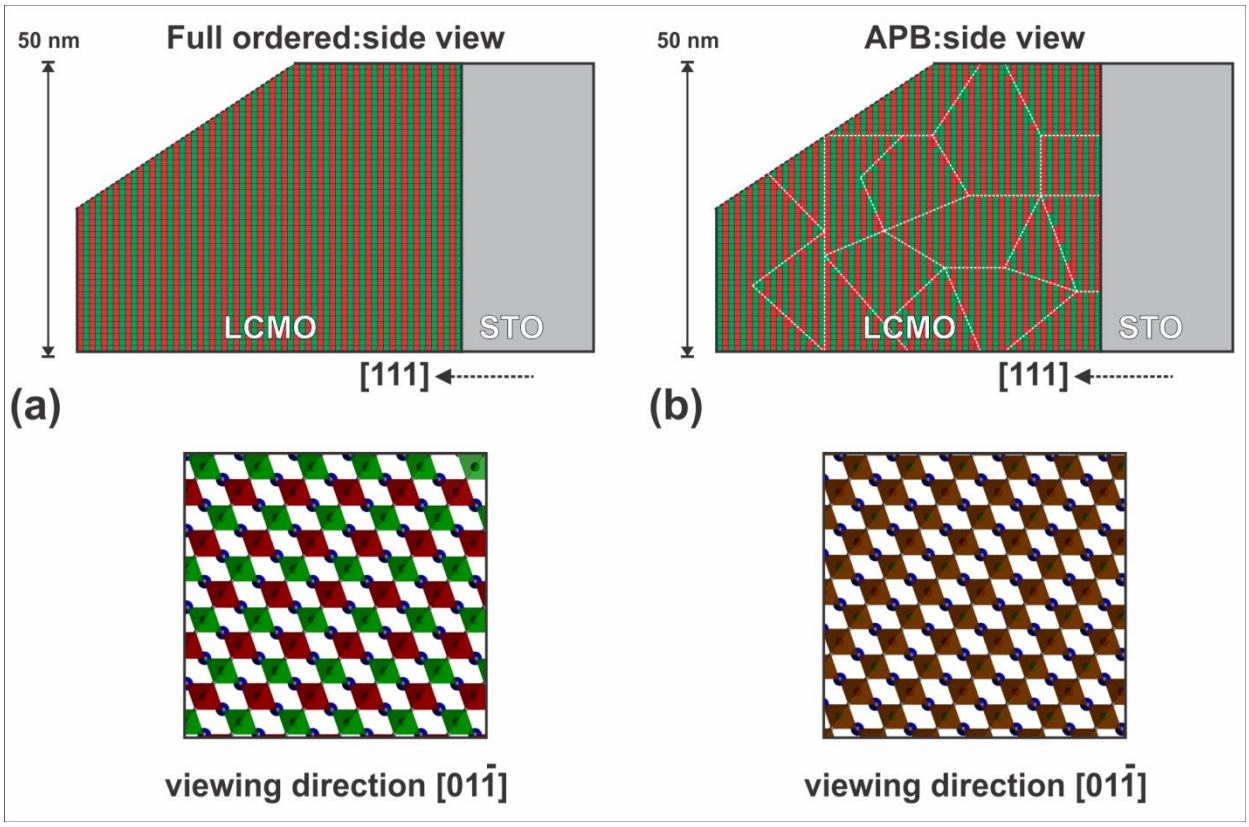


Fig. 6: A sketch of the proposed (a) well-ordered and (b) suppression of the B-site ordering due to phase-shifted ordered domains of finite size, marked by white lines (short range ordering). The thickness profile of the TEM lamella as estimated by EELS from the log-ratio technique is approximately 25 nm (at the top surface) and 50 nm closer at the film/substrate interface. Hence, the probability to find an ordered region is larger for the surface region of the sample as for the interface. Schematic visualization of the B-site ordering for both (a) well-ordered thin film and (b) the apparent disorder created as a result of the superimposing ordered domains, along the viewing direction. The color scheme follows: Manganese (red), Cobalt (green), La (blue) and Co/Mn (disordered, brown). The [111] arrows indicate the growth direction of the film.

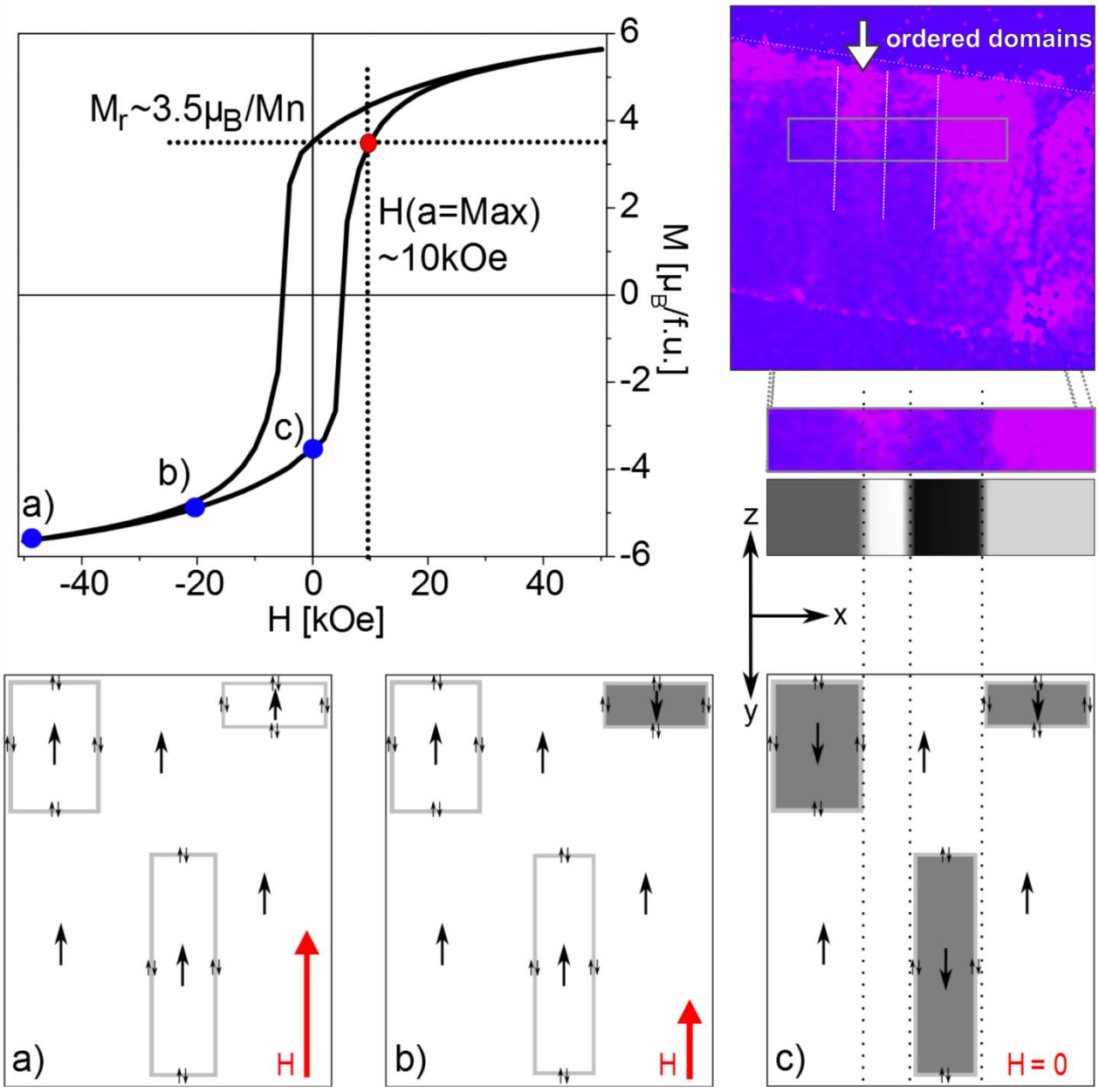


Fig. 7: A model of the magnetization of anti-phase-domains (APDs) separated by antiferromagnetic APBs ($^1/_2\,^1/_2\,^1/_2$)/(111) intensity ratio map, obtained by Fourier filtering of a high resolution HAADF image, shows intensity differences in the x-z-plane. This can be interpreted as APDs in the x-y-plane, in which the purple areas correspond to areas with a small volume amount of APDs. The blue areas represent areas with a large volume fraction of APDs. APDs have impact on the magnetism: a) nearly all domains are aligned parallel to the external field close to the saturation field b) for moderate fields the magnetization of small domains flips antiparallel to the applied field; c) all APDs are antiferromagnetically coupled to the surrounding phase-shifted material for zero external field, H=0. The blue dots mark the positions of the states with different applied external field in the hysteresis loop of the LCMO film. Considering a similarity between the reversed low field (H<0) and the remanent (H=0) magnetization (the red dot in the hysteresis loop) the field, which is necessary to flip the biggest APD, can be estimated to H~10kOe.